Research Article | Vol. 30, No. 15 / 18 Jul 2022 / Optics Express 27164
Optics EXPRESS

Two-photon interference LiDAR imaging

ROBBIE MURRAY AND ASHLEY LYONS*

School of Physics and Astronomy, University of Glasgow, Glasgow, G12 8QQ, UK
*ashley.lyons@glasgow.ac.uk

Abstract: Optical Coherence Tomography (OCT) is a key 3D imaging technology that provides micron scale depth resolution for bio-imaging. This resolution substantially surpasses what it typically achieved in Light Detection and Ranging (LiDAR) which is often limited to the millimetre scale due to the impulse response of the detection electronics. However, the lack of coherence in LiDAR scenes, arising from mechanical motion for example, make OCT practically infeasible. Here we present a quantum interference inspired approach to LiDAR which achieves OCT depth resolutions without the need for high levels of stability. We demonstrate depth imaging capabilities with an effective impulse response of 70 μm, thereby allowing ranging and multiple reflections to be discerned with much higher resolution than conventional LiDAR approaches. This enhanced resolution opens up avenues for LiDAR in 3D facial recognition, and small feature detection/tracking as well as enhancing the capabilities of more complex time-of-flight methods such as imaging through obscurants and non-line-of-sight imaging.

1. Introduction

Optical Coherence Tomography (OCT) is a 3D imaging approach whereby depth information is obtained from the interference of short coherence length light sources [1]. It is employed in a wide variety of bio-imaging applications perhaps most notably in ophthalmology, but also including and not limited to cardiology, oncology, and dermatology [2–6], owing to its ability to image within scattering media. Each interface inside a medium, usually a biological tissue, creates a reflection which interferes with a reference field. The location of the envelope function for each of these interference maxima is used to discern the distance light has propagated, or equally the Time-of-Flight (ToF), and thus the depth within the medium. In this way axial resolutions on the micron scale are routinely achieved with less than 1 μm having been demonstrated [7,8].

OCT is dependent on the observation of the interference fringes arising from the cyclic phase of the optical field (regardless of whether they are observed in the temporal or spectral domain) and is thus an inherently coherent process. It is therefore not readily extended to incoherent systems e.g. situations where there is a mechanical movement on the wavelength scale or greater over the course of the acquisition time. These circumstances are abundant in LiDAR (Light Detection and Ranging) where interferometric stability cannot be achieved and even fluctuations in air currents can cause a substantial phase distortion. Conventional single photon LiDAR is typically limited by the timing jitter of the detector which is on the order of tens of picoseconds or greater for SPADs [9], resolving depth profiles on the millimetre scale and below therefore proves to be challenging.

Hong-Ou-Mandel interferometry [10] presents similar capabilities and the same depth resolution but in a way which is incoherent where we define "incoherent" as possessing no first order coherence i.e. no dependence on the optical phase. For this reason, schemes based on HOM interferometry have been referred to as "Quantum OCT" (QOCT) in the literature [11,12]. QOCT instead gains ToF information by examining photon bunching at the output ports of an interferometer, usually by measuring correlated events between two single photon detectors,

#461248 https://doi.org/10.1364/OE.461248
Journal © 2022 Received 19 Apr 2022; revised 10 Jun 2022; accepted 15 Jun 2022; published 13 Jul 2022

Optics EXPRESS

and mapping the envelope function directly without the need for phase dependent fringes. Recent works have shown how depth resolutions down to the sub-nanometre scale with HOM interferometry whilst also bypassing the need for any scanning elements [13].

QOCT instead faces another challenge, HOM interferometry uses precisely 1 photon in each arm of the interferometer: one which is sent to the scene and the back-scattered light collected that we refer to as “probe" and the other kept in a controlled delay line that we refer to as “reference", this is usually achieved with Spontaneous Parametric Down Conversion (SPDC). These sources a limited to at most 1 photon pair per pump laser pulse to remain in a photon starved regime and thus maintain high interference visibility. Where there are significant losses, this proves detrimental and cannot be mitigated by e.g. increasing the number of photon pairs without also introducing other negative effects such as limiting the non-ambiguous range of a LiDAR system. By way of example, consider SPDC photon pairs being generated at a rate of 10MHz with a loss rate of 10^6 (60 dB), only 10 coincident events per second would remain detectable. The generation rate could be increased to e.g. 1 GHz allowing 1,000 events to be measured per second but the range would be then limited to 30 cm. An equivalent of QOCT using classical states of light has also been demonstrated in the form of Chirped Pulse Interferometry (CPI) where benefits such as dispersion cancellation can be achieved without relying on entangled photon pairs [14]. Interference between pairs of frequency combs has been used to achieve a similar goal, however requiring the use of a pair of femtosecond laser systems [15]. In addition to QOCT, there are a range of alternative schemes that combine interferometry with photon pair correlation measurements [16,17].

In the following, we explore the potential for using two-photon interference between weak coherent states of light specifically for LiDAR applications where it can provide the micron-scale depth resolution of OCT whilst also being immune to phase noise and able to operate in high loss environments. As well as demonstrating imaging capabilities for the first time, we investigate limitations on the achievable depth resolution and propose a new method for increasing the number of photon correlation resources to decrease the acquisition time. In the final sections of the article we discuss routes towards building a real-time imaging scheme based on this principle.

2. Experimental layout

To demonstrate the concept, we construct a system (depicted in Fig. 1(B)) using a Ti:Saph oscillator (Coherent Chameleon Ultra II) with pulse duration of 130 fs at a rate of 80 MHz and a centre wavelength of 810 nm. This is split into two arms of roughly equal intensity to act as the reference and probe arms of the interferometer. The reference arm is coupled into a polarisation maintaining single mode fiber mounted on a translation stage to control the optical delay. The probe arm is also coupled into fiber before being directed onto a pair of scanning mirrors for transverse image scanning and the phase is randomised using a piezo actuator. The returned light is collected with the same optics and coupled back into single mode fiber before being combined with the reference arm at a fiber coupled beamsplitting cube. The use of single mode fibers (and a fiber-coupled beamsplitter) maximises the spatial mode overlap of two interferometer arms at the final beamsplitter and therefore the interference visibility. The photon number from each of the interferometer arms is further controlled and balanced using neutral density filters. The two output ports of the interferometer are measured using single pixel SPADs and the number of correlated photon pair events is measured using a TCSPC module (ID Quantique ID801). To demonstrate our system’s high depth resolution, we acquire a depth scan of the two reflective surfaces of a 2mm thick glass diffuser (see Supplementary Material). Here, a deeply sub-mm depth response can readily be observed.

Optics EXPRESS

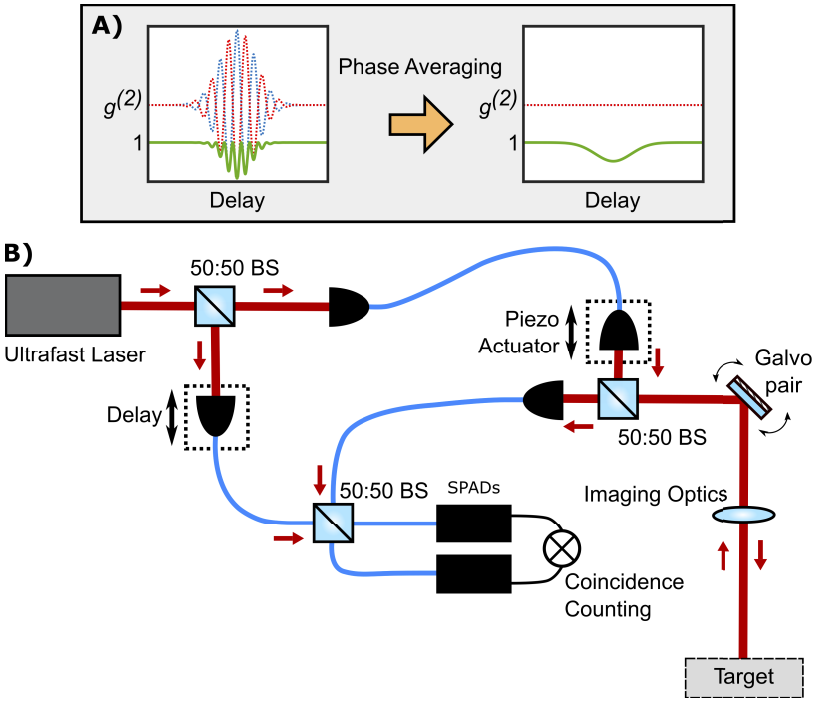

Fig. 1. A) Illustration of the working principle for the Two-Photon Interference LiDAR concept. The second order correlation function, $g^{(2)}$, from the two output ports of an interferometer are measured (green). Intensity of the two ports are also shown (red & blue dashed). When there is a large amount of phase noise (Phase Averaging) the envelope function remains in the $g^{(2)}$. B) Schematic diagram of the experimental setup. Red arrows indicate beam propagation direction. From the first beamsplitter (50:50 BS), one arm of the interferometer (top left) is sent to the scene through a scanning mirror pair. The returned light is collected with a single mode fiber. The other arm (bottom right) is collected with a fiber with control over the optical path length (Delay). The phase of the interferometer is continuously randomised by a piezo actuator in one of the two arms. The two arms meet at a beamsplitter and where the output ports are monitored by a pair of SPADs.

3. High resolution 3D imaging

Full 3D imaging is performed by scanning the beam in the transverse plane using the galvanometer mirror system. Collimation optics are fixed in front of the illumination and collection fibers and the far-field of the scanning mirrors is imaged onto the scene, positioned 1 m away, by a single lens. The scene is scanned in a grid of 100×100 positions and the depth is estimated by taking the center position of a Gaussian function fitted to each delay scan, details of which can be found in the Supplementary Material. We find that the depth resolution for our system, estimated from the uncertainty in the $g^{(2)}$ minimum position from our fits, to be approximately 7 μm.

The resulting depth map for a scene consisting of a 20 pence coin is shown in Fig. 2. We can determine an effective IRF for our system from the width of the correlation dip where, in the specific case of Fig. 2, we measure this to be 70.4 μm. The depth scan was achieved using 75 steps with a 50 ms integration time per point, giving a total acquisition time for the image of approximately 10 hours.

Due to the high depth resolution (or equivalently, time-of-flight resolution) this method is capable of, and the relatively large distances of interest to LiDAR, small path length differences

Optics EXPRESS

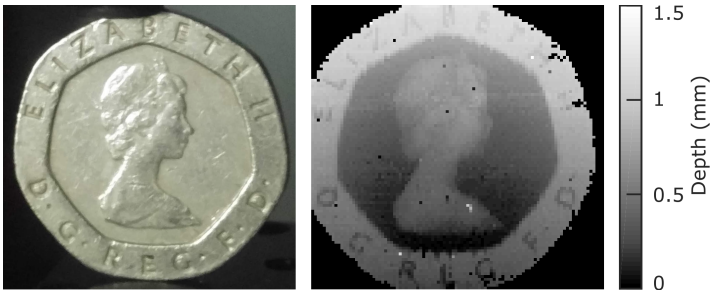

Fig. 2. Experimental demonstration of imaging two-photon interference LiDAR. Photograph of sample (left) and measured depth map (right) of a 20 pence coin. Estimated depth resolution is 7 μm.

owing to the geometry of the scene must be taken into account as they produce not only a transversely dependent offset to the photon time of arrival but will also effect the axial resolution. At a given stand-off distance from the scene, the spot size of the transverse scanning system (or equally the transverse resolution for a full-field system) acts as an additional source of axial uncertainty with larger spots producing a greater spread of arrival times. At a given distance, Z, transverse spot radius, r_{spot}, and pulse duration, τ_{pulse}, the depth uncertainty can be approximated as

$$\Delta Z = \sqrt{\left(\sqrt{Z^2 + r_{\text{spot}}^2} - Z\right)^2 + 2\tau_{\text{pulse}}^2}. \tag{1}$$

This effect is numerically estimated in Fig. 3(A) for a stand-off distance of 10 m and a pulse duration of 100 fs. As expected, for small spot sizes, the axial (depth) resolution is limited by the duration of the optical pulse. However, for beam diameters greater than 10 mm the geometric uncertainty becomes visible and scales as r_{spot}^2. The impact of the transverse spot size on the axial resolution reduces as the distance to the scene is increased: Fig. 3(B) shows the required transverse resolution as a function of the standoff distance to achieve axial resolutions of 50, 100, 500, and 1000 μm. This is due to a parallax effect whereby the difference in path length from the sensor to one transverse extreme point in the scene, and the sensor at the other extreme, decreases.

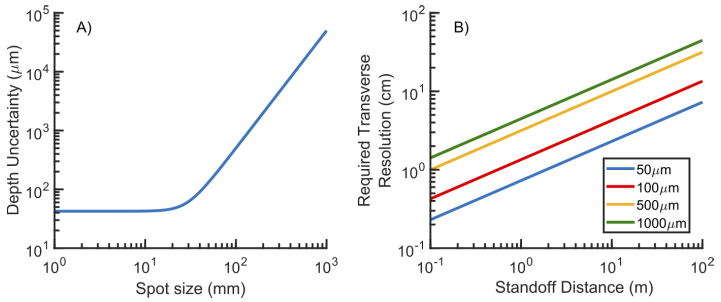

Fig. 3. A) Numerical estimation of the axial resolution as a function of transverse resolution for a fixed standoff distance of 10 m and pulse duration 100 fs. B) The minimum required transverse resolution to achieve a given depth resolution for the same 100 fs pulse.

Optics EXPRESS

4. Photon number and loss

We evaluate the losses and compare to QOCT and other methods that rely on correlation between photon pairs from e.g. SPDC. Here we assume a loss that scales linearly with propagation distance as will occur in schemes where only one of the two photons is sent to the scene. Using a diffuser (see SM) as an example of realistic backscattering conditions (FWHM of scattering cone $\approx 16^\circ$ from specification) and a distance of 100 m, a 2 inch optic would only be able to collect approximately 2×10^{-4} % of the returned light (56 dB loss). An SPDC source generating on the order of 10^6 photon pairs per second would therefore only be able to measure 1-2 correlated events within the time used to acquire a single temporal scan from the experiment shown here (3.75 s). Where, with the proposed Two-Photon Interference LiDAR method this loss is compensated by simply increasing the laser power, generating more photon pairs via optical nonlinearities without also introducing substantial numbers of multi-pair events remains a significant technical challenge.

We note that, due to the use of coherent states as opposed to photon pairs from SPDC, correlated events need not be limited to photons from the same optical pulse. Consider a scene that is imaged using pulses at a repetition rate on the MHz scale that only exhibits phase noise on the kHz scale, pulses within a 1μs window of each other observe the same interferometer phase and therefore the same behaviour will be seen in the $g^{(2)}$ regardless of whether correlations are taken between pairs of photons from different pulses within this timescale or the same pulse. To demonstrate how this can be exploited we conduct an additional measurement where we record the individual timetags of each detected photon and examine correlations between neighbouring pulses up to a decorrelation time τ_{corr}. The total number of correlated events in this time can then be summed resulting in a vast increase in the total number of photon counting resources from the same physical measurement, thereby also allowing the measurement time to be decreased whilst maintaining the same SNR. We find that, for our specific system, up to the closest 1000 pulses can be used within the time τ_{corr} allowing for an acquisition time three orders of magnitude faster. A comparison of a correlation dip with and without our method can be seen in Fig. 4. Full details of this approach can be found in the Supplementary Materials.

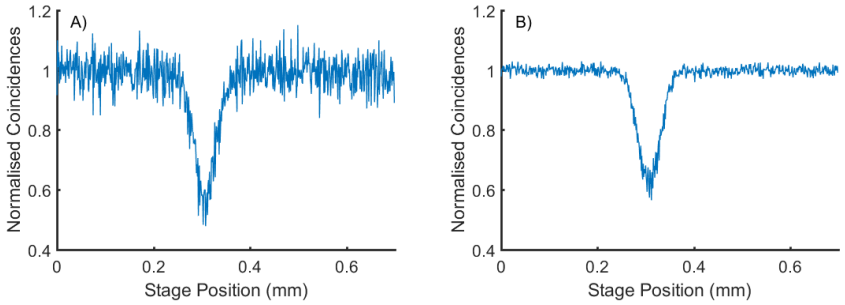

Fig. 4. Improvement in the noise of the correlation dip using our approach. A) The standard approach to measuring correlated events where a coincidence is registered when a photon arrives at both detectors on the same pulse. B) The dip recovered using our method looking at correlations between, in this case, the closest 1000 pulses.

5. Discussion

In our measurements, we use prior knowledge about the object position to limit the scan length and therefore overall measurement time. We note, however, that the approximate position of objects of interest in the scene can be instead gained using conventional single photon LiDAR as all the same components are present here (pulsed laser, single photon detector, TCSPC). The axial

Optics EXPRESS

resolution demonstrated here can be increased further by the use of pulses of shorter duration. It then also becomes important to consider the effects of chromatic dispersion from propagation within the air and fibers which will broaden the pulse. We note, however, that the 100 fs pulse discussed here will only broaden by around 14 fs for 100 m propagation in air due to second order dispersion [18,19]. This can be compensated within either the signal or reference arm and could be optimised without any prior knowledge of the propagation distance. Although the measurement shown in Fig. 2 required over 10 hours to acquire, this can be greatly reduced by using our proposed multiple-pulse correlation method to just 36 s. Further improvements can be achieved by the removal of the transverse scanning elements in favour of a full-field imaging system. Full-field OCT is routinely performed and it is only the addition of the correlation measurements that would be required to extend this to the approach presented here. To achieve this, cameras which are able to distinguish $g^{(2)}$ from individual photon correlations at a high rate is preferable. Recent advancements using SPAD cameras have proven to be a promising candidate for this [20]. Full-field imaging with HOM interference has been recently demonstrated using SPAD cameras, the scheme however relied on the spatial correlation between photon pairs from an SPDC source [21]. The same method can be adapted for our LiDAR scheme by using spatially correlated light sources.

6. Conclusions

We demonstrate a new method for LiDAR using intensity correlation based interferometry with the depth resolution of an OCT system. We have shown imaging capabilities with the ability to discern two different depth objects at the same pixel down to separations of 70 μm. Our approach has applications not only for high-precision LiDAR, but also in other ToF sensing systems where one wishes to measure the full temporal distribution of light pulses with high resolution such as imaging through scattering media and Non-Line-of-Sight imaging.

Funding. Engineering and Physical Sciences Research Council (EP/R030081/1); Royal Academy of Engineering (RF\202021\20\329).

Acknowledgements. The authors acknowledge support from the Royal Academy of Engineering and EPSRC.

Disclosures. The authors declare no conflicts of interest.

Data availability. Data used to produce all figures shown in this paper can be found at [22].

Supplemental document. See Supplement 1 for supporting content.

References

1. D. Huang, E. Swanson, C. Lin, J. Schuman, W. Stinson, W. Chang, M. Hee, T. Flotte, K. Gregory, C. Puliafito, and A. Et, "Optical coherence tomography," Science **254**(5035), 1178–1181 (1991).
2. J. G. Fujimoto, C. Pitris, S. A. Boppart, and M. E. Brezinski, "Optical Coherence Tomography: An Emerging Technology for Biomedical Imaging and Optical Biopsy," Neoplasia **2**(1-2), 9–25 (2000).
3. J. Welzel, "Optical coherence tomography in dermatology: a review," Ski. Res. Technol. **7**(1), 1–9 (2001).
4. A. M. Zysk, F. T. Nguyen, A. L. Oldenburg, D. L. Marks, and S. A. Boppart, "Optical coherence tomography: a review of clinical development from bench to bedside," J. Biomed. Opt. **12**(5), 051403 (2007).
5. T. Yonetsu, B. E. Bouma, K. Kato, J. G. Fujimoto, and I.-K. Jang, "Optical Coherence Tomography," Circ. J. **77**(8), 1933–1940 (2013).
6. X. Shu, L. Beckmann, and H. F. Zhang, "Visible-light optical coherence tomography: a review," J. Biomed. Opt. **22**(12), 1 (2017).
7. E. Bousi, I. Charalambous, and C. Pitris, "Optical coherence tomography axial resolution improvement by step-frequency encoding," Opt. Express **18**(11), 11877 (2010).
8. A. Lichtenegger, D. J. Harper, M. Augustin, P. Eugui, M. Muck, J. Gesperger, C. K. Hitzenberger, A. Woehrer, and B. Baumann, "Spectroscopic imaging with spectral domain visible light optical coherence microscopy in Alzheimer's disease brain samples," Biomed. Opt. Express **8**(9), 4007 (2017).
9. M. Sanzaro, P. Gattari, F. Villa, A. Tosi, G. Croce, and F. Zappa, "Single-Photon Avalanche Diodes in a 0.16 μm BCD Technology With Sharp Timing Response and Red-Enhanced Sensitivity," IEEE J. Sel. Top. Quantum Electron. **24**(2), 1–9 (2018).
10. C. K. Hong, Z. Y. Ou, and L. Mandel, "Measurement of subpicosecond time intervals between two photons by interference," Phys. Rev. Lett. **59**(18), 2044–2046 (1987).

Optics EXPRESS

11. A. F. Abouraddy, M. B. Nasr, B. E. A. Saleh, A. V. Sergienko, and M. C. Teich, "Quantum-optical coherence tomography with dispersion cancellation," Phys. Rev. A **65**(5), 053817 (2002).
12. M. B. Nasr, D. P. Goode, N. Nguyen, G. Rong, L. Yang, B. M. Reinhard, B. E. Saleh, and M. C. Teich, "Quantum optical coherence tomography of a biological sample," Opt. Commun. **282**(6), 1154–1159 (2009).
13. A. Lyons, G. C. Knee, E. Bolduc, T. Roger, J. Leach, E. M. Gauger, and D. Faccio, "Attosecond-resolution Hong-Ou-Mandel interferometry," Sci. Adv. **4**(5), eaap9416 (2018).
14. J. Lavoie, R. Kaltenbaek, and K. J. Resch, "Quantum-optical coherence tomography with classical light," Opt. Express **17**(5), 3818 (2009).
15. H. Wright, J. Sun, D. McKendrick, N. Weston, and D. T. Reid, "Two-photon dual-comb LiDAR," Opt. Express **29**(23), 37037 (2021).
16. R. Chrapkiewicz, M. Jachura, K. Banaszek, and W. Wasilewski, "Hologram of a single photon," Nat. Photonics **10**(9), 576–579 (2016).
17. H. Defienne, B. Ndagano, A. Lyons, and D. Faccio, "Polarization entanglement-enabled quantum holography," Nat. Phys. **17**(5), 591–597 (2021).
18. I. Walmsley, L. Waxer, and C. Dorrer, "The role of dispersion in ultrafast optics," Rev. Sci. Instrum. **72**(1), 1–29 (2001).
19. P. J. Wrzesinski, D. Pestov, V. V. Lozovoy, J. R. Gord, M. Dantus, and S. Roy, "Group-velocity-dispersion measurements of atmospheric and combustion-related gases using an ultrabroadband-laser source," Opt. Express **19**(6), 5163 (2011).
20. B. Ndagano, H. Defienne, A. Lyons, I. Starshynov, F. Villa, S. Tisa, and D. Faccio, "Imaging and certifying high-dimensional entanglement with a single-photon avalanche diode camera," npj Quantum Inf. **6**(1), 94 (2020).
21. B. Ndagano, H. Defienne, D. Branford, Y. D. Shah, A. Lyons, N. Westerberg, E. M. Gauger, and D. Faccio, "Quantum microscopy based on hong–ou–mandel interference," Nat. Photonics **16**(5), 384–389 (2022).
22. A. Lyons, "Associated dataset," University of Glasgow (2022) http://dx.doi.org/10.5525/gla.researchdata.1306 .